Blast Response of Segmented Bored Tunnel using Coupled SPH-FE Method

Sivalingam Koneshwaran, David P. Thambiratnam*, Chaminda Gallage

Science & Engineering Faculty, Queensland University of Technology, Brisbane, Australia.

Abstract

Underground transport tunnels are vulnerable to blast events. This paper develops and applies a fully coupled technique involving the Smooth Particle Hydrodynamics and Finite Element techniques to investigate the blast response of segmented bored tunnels. Findings indicate that several bolts failed in the longitudinal direction due to redistribution of blast loading to adjacent tunnel rings. The tunnel segments respond as arch mechanisms in the transverse direction and suffered damage mainly due to high bending stresses. The novel information from the present study will enable safer designs of buried tunnels and provide a benchmark reference for future developments in this area.

Key words: explosion; finite element method; smooth particle hydrodynamics; segmented tunnel; dry soil,

1. Introduction

The scarcity of above ground space has resulted in a surge in the construction of buried transportation tunnels in urban environments. As a large number of people use these transportation tunnels on a daily basis, they could be prime targets for terrorist attacks. Recent events such as the Boston Bombings of 2013 highlight the importance of continued vigilance towards terrorist attacks. In particular, blast impact on transportation tunnels must be closely considered for two reasons; i) the importance and centrality of such infrastructure, and ii) the level of public use. The failure of such underground tunnels would not only cause delays and transport network interruptions but also result in severe loss of lives with considerable financial implications. Transportation tunnels must therefore be designed to mitigate the adverse effects of credible blast events.

* corresponding author: tel: 61 7 31381467; fax: 61 7 3138 1170; e-mail: d.thambiratnam@qut.edu.au

Internal blasts have been considered in the past by many researchers [1-4], however, these would seem to be less likely. It is difficult to place an explosive device within a tunnel and having a moving vehicle filled with explosives is not feasible in subway systems. Surface blasts are the most likely events and have the potential to cause most damage. Tunnels are essentially constructed at shallow depths just below the ground in the built environment and they are most likely to suffer damage caused by surface explosions. Furthermore, due to the crowded nature of underground developments, the failure of a buried tunnel caused by blast loading will increase the risk of failure of above ground structures in the area.

Some tunnels are designed to withstand natural disaster events such as earthquakes or fire, but most tunnels are not designed to withstand blast loading[4]. This highlights the need to investigate the vulnerability of transit tunnels to credible blast loading. Conducting a full-sized tunnel test is extremely risky and expensive in this research field. However, some researchers have treated the tunnel response under surface blast using scaled-down centrifuge modeling and explicit nonlinear finite element techniques.

Geotechnical centrifuge modeling provides a valid technique to test models in geotechnical problems. Many researchers [5-10] have successfully employed the centrifuge modeling to simulate the blast response of buried structures. De et al. [5, 6] describe a recent series of centrifuge tests to study the surface blast effect on buried copper pipe in dry sand. In the centrifuge test, the gravitational acceleration increases with radial distance of the rotating arm. As a result, the gravitational field is not constant across its depth of the model. This limitation in the centrifuge test restricts the testing to smaller models.

Reinforced concrete is still the principal construction material for transportation tunnels. Transportation tunnels are mostly bored tunnels which consist of several precast segmented linings which create a system with multiple joints or hinges. Scaled-down modeling of large reinforced concrete structures in the centrifuge may be impossible due to the size limitation. It may be even more difficult to investigate the effect of interaction of adjacent segments in the tunnel. Although the study by De et al. [5, 6] provides some overall quantitative information on the blast response of a buried tunnel, it is unable to provide detail information on segmental behaviour of a buried tunnel and effects of reinforcement as a copper pipe was

used in the experiments. Hayes [11] considered the Conventional Weapon Effects Backfill (CONWEB) test series to investigate the blast response of a reinforced concrete structure buried in various backfill soil conditions. The study was conducted with a small scale full-sized model which considered the interaction of two sub structures connected by bolts. Given this information, the combination of these two experiments provides a means for validating numerical methods, particularly under blast modeling, where full-sized tests are often impractical.

Some researchers [1-3, 6, 12, 13] treated the transportation tunnel under blast using different numerical techniques. De [6] conducted a three dimensional numerical simulation of surface blast induced tunnel response using ANSYS Autodyn. The study used fluid-structure interaction with a default sand model [14] to simulate a dry sand and the simulation was validated with his centrifuge test results. Yang et al. [12] investigated the blast response of a metro tunnel in Shanghai using an advanced general purpose multi-physics computer software LS-DYNA [15]. The study employed Arbitrary Lagrangian Eulerian (ALE) method with merged nodes between Eulerian soil meshes and Lagrangian tunnel meshes. The other two materials, air and explosive, were modeled as Eulerian meshes. This simulation failed to incorporate the ground-lining interaction by merging the nodes as separation, re-contact and sliding are possible at the contact interface. These studies have all ignored the important aspect of segment joints. Nasri Munfah [4] stated that a thin precast segmented tunnel lining is more vulnerable to blast than thick cast in place tunnels. Under geo-static conditions, segmented tunnel linings allow a degree of rotation at contact joints without significant loss of load bearing capacity. However, as a result of blast, differential movement between tunnel segments, loss of contact and ground-lining interaction change the mode of load transfer at the contact joints.

This paper develops and applies a fully coupled technique involving the Smooth Particle Hydrodynamics (SPH) and Finite Element Method (FEM) for investigating the blast response of segmented bored tunnels. To the best of the authors' knowledge, this study is the first of its kind to treat the blast response of segmented buried tunnels. The commercially available non-linear finite element software package LS-DYNA is used in this study. The SPH particles are used to model the explosive and the soil that experience large deformations, while the Finite elements (FE) are used to model the rest of the soil and the tunnel. Inclusion of pore water

effects in the soil can have a significant influence on the response of buried tunnels to blasts as commented by other researchers such as De [6] who recommended that pore water effects be incorporated in the soil model. The present study address this issue and utilizes the *MAT_FHWA_SOIL material model which is capable of simulating dry, partially saturated and fully saturated soil conditions.

2. The Coupled SPH-FEM

SPH is a mesh-free computational Lagrangian hydrodynamic particle method. This method originated about three decades ago in astrophysical problems [16, 17], where it dealt with the simulation of interacting fluid masses in vacuum without boundaries. It was then modified as a deterministic mesh-free particle method and implemented to continuum solid and fluid mechanics [18, 19]. SPH treats the solid mechanics problems in which large deformations and fragmentation occur. SPH is mathematically based on interpolation theory by utilizing kernel approximation of a function which is adequately smooth even for higher order derivatives and provides stable and accurate results. When SPH was initially implemented to fields other than astrophysics, it suffered from the enforcing of finite boundary conditions. Modeling of FEM meshes as boundaries for SPH particles offers a possible solution [20].

SPH provides extensive ability as a numerical tool for modeling problems having large distortions and deformations. Unlike conventional Lagrangian meshing, SPH is free from mesh tangling and hour-glassing effects. As such, SPH particles are used where large deformation or severe material failure occurs in near field domain and FEM meshes are used where intermediate or small deformation is expected in far field domains.

Although SPH is more expensive in terms of computation, the coupled SPH-FEM approach reduces high computational demand. There are methods that allow the coupling interaction between SPH particles and FEM meshes [21]. A constraint interface ties SPH particles to the corresponding surfaces of FEM meshes as shown in Figure 1(a). This method requires due consideration in FEM mesh creation at the interface as it could cause un-physical penetration and system instability. Hybrid element coupling is a new feature in LS-DYNA. As shown in Figure 1(b), these elements constrain SPH particles and act as transit layers between SPH particles and FEM meshes. The main advantage of this method is that no tied/contact

interface is required. However, this method suffers from intruding SPH particles into FEM mesh if hybrid elements are close to the explosive. The third method is a simple method where the interaction is achieved by the penalty based 'Nodes-to-surface' contact where solid elements as the master and SPH particles as the slave nodes as shown in Figure 1(c). The 'Node-to-surface' coupling method is employed in the present study as SPH particles are close enough to achieve steady interface.

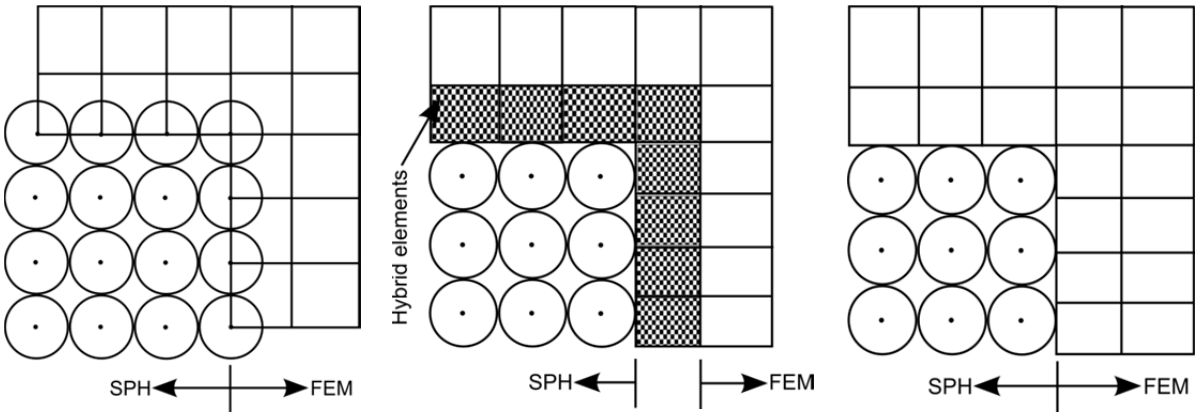

a) Tied interface b) Hybrid element coupling c) 'Nodes-to-surface' contact

Figure 1: Coupled SPH-FEM

3. Material Constitutive Models

This paper studies the blast response of a bored tunnel with segmented tunnel lining using the non-linear Finite Element code LS-DYNA. For validation purpose, experiments reported by De [6] and Hayes [11] are simulated using the coupled SPH-FEM. The following material constitutive models are utilized for the simulation;

3.1. Explosive

A popular equation utilized in SPH simulation is the Jone-Wilkin-Lee (JWL) Equation of State (EOS). The JWL EOS defines the pressure ***P*** as a function of the relative volume (or the expansion of the explosive) ***V***, and initial energy per volume ***E*** in the detonation of explosives as:

$$P = A\left(1 - \frac{\omega}{R_1 V}\right)e^{-R_1 V} + B\left(1 - \frac{\omega}{R_2 V}\right)e^{-R_2 V} + \frac{\omega E}{V} \qquad \text{Eq. 1}$$

In the above equation ***A, B, R_1, R_2*** and ***ω*** are the empirically derived constants for the explosive. Table 1 shows the material parameters used for both TNT (Trinitrotoluene) [21] and C-4 [22] explosives.

Table 1: Material parameters for TNT explosive

Parameters	TNT	C-4
ρ (g/cm^3)	1.630	1.601
v_D (m/s)	6930	8193
PCJ (GPa)	21	28
A (GPa)	373.77	609.97
B (GPa)	3.747	12.95
R_1	4.15	4.5
R_2	0.90	1.4
ω	0.35	0.25
V	1	1
E0 (kJ/ m^3)	6.0e+06	9.0e+06

3.2. Soil

There are several soil material models available in LS-DYNA, but selection of an appropriate soil model is essential in the blast simulation to accurately transmit the shock wave in the soil. *MAT_FHWA_SOIL model was identified as a suitable model that incorporates strain softening, kinematic hardening, strain rate effects, element deletion, excess pore water effects and stability with no soil confinement [23, 24]. The material model was developed by the Federal Highway Administration (FHWA) in 2004 to investigate the dynamic response of road safety barriers on the ground. The FHWA soil model is based on a modified Mohr-Coulomb yield criterion [25]. The modified yield surface is a smooth hyperbolic surface which allows an accurate, robust, and saving of computational demand of the numerical simulation.

The FHWA soil model needs main parameters such as, mass density, specific gravity, bulk modulus, shear modulus, friction angle, cohesion and moisture content. These soil parameters are commonly determined from laboratory tests. Parameters required for describing strain softening, kinematic hardening, strain rate effects and pore water effects can be evaluated from laboratory tests and/or equations in the manual [23].

Researchers Jayasinghe et al.[26], Lee [27] and Ortman [28] have successfully employed this model for studying blast effect in fully saturated soil by considering the pore-water effect. The same model can be utilized by eliminating pore-water effects if the soil is unsaturated or dry [23, 27]. Values recommended by Lee [27] were used in this paper to incorporate the strain softening, kinematic hardening and strain rate effects in the soil.

3.2.1. Dry Nevada sand

De [6] used Nevada dry sand (at a relative density (D_r) of 60%) to investigate the blast response of a buried copper pipe. The soil parameters were evaluated from different studies. VELCS (Verification of Liquefaction Analyses by Centrifuge Studies) Program [29] provides the main soil properties such as mass density and specific gravity. Based on Poisson's ratio of 0.33 and sound speed of 301 ms^{-1} [6], shear and Bulk moduli were calculated and are presented in Table 2. The calculated shear modulus is consistent with the shear modulus evaluated from resonant column test [29].

3.2.2. Partially saturated sand in a backfill test

In the CONWEB test series, Hayes [11] considered a high shear strength and low seismic velocity compacted concrete sand in backfill Test 3. The soil properties such as density, specific gravity and water content are shown in Table 2. The shear and bulk moduli were evaluated based on the density, seismic velocity and Poisson's ratio [30]. The calculated bulk modulus is consistent with the volumetric strain changes observed between pressure steps [31]. The cohesion and friction angle were based on the modified material properties described by Baylor [31].

To include the pore-water effects in the soil model, the parameters PWD_1, PWD_2 and K_{sk} should be active in the input material card [23]. PWD_1 defines the stiffness of the soil by

adjusting the bulk modulus before the air voids collapse. PWD_2 calculates the pore-water pressure in the soil before the air voids collapse. As suggested by Lee [27], K_{sk} is the volumetric strain factor which varies between 5% and 20% of material bulk modulus. Degree of saturation of the sand was evaluated as 26% based on the density, specific gravity and water content. PWD_2 was determined for partially saturated soils using the equation in reference [23]. PWD_1 was estimated based on best fit material analysis graph using the free-field blast simulation reported in Section 5.2.

Table 2: Material parameters for soil

Parameters	Dry Nevada sand	Compacted concrete sand
Density (g/cm^3)	1.60	1.865
Specific gravity	2.67	2.70
Shear modulus (MPa)	56.0	70.2
Bulk modulus (MPa)	146.0	117.0
Cohesion (MPa)	6.20e-03	3.723e-2
Friction angle	35^o	40^o
Moisture content (%)	0	5.0
PWD_1 (MPa^{-1})	0	2.500e-02
PWD_2(MPa^{-1})	0	1.152e-02

3.3. Concrete

Although LS-DYNA material library has several advanced constitutive material models developed to simulate concrete material behavior, selection of a model capable of characterizing concrete performance under blast load is very essential. In many circumstances, the necessary material parameters for the concrete cannot be found in the literature. This study utilized two most common material models: *MAT_CONCRETE_DAMAGE Rel. III (Mat_Rel3) [32] and *MAT_WINFRITH_CONCRETE (Mat_winfr) [15], which have the automatic generation capability of concrete law parameters.

The material model Mat_Rel3 works with the two input parameters, concrete density and the unconfined compressive strength. If the simulated response shows a significant difference from the observed performance of the concrete, the material parameters can be refined [32, 33]. This model includes three failure surfaces, such as maximum failure surface, initial yield surface and residual failure surface, to correlate the stress-strain relationship of the material. Furthermore, strain rate effects due to high dynamic loading were added in the model as a dynamic increase factor (DIF) described by Malvar et al. [34].

Table 3: Material parameters for concrete

Parameter	Test slab (Test 3)	
	Mat_Rel3	Mat_084/085
Density (g/cm3)	2.24	2.24
Tangent modulus (GPa)	_	28.8
Unconfined compressive strength (MPa)	40.4	40.4
Poisson's ratio	0.19	0.19
Uniaxial tensile strength (Mpa)		3.54
Fracture energy per unit area (N/m)	_	70.0
Maximum aggregate size (mm)	9.5	9.5

The material model Mat_winfr is another simple input concrete model which requires the unconfined compressive strength and tensile strength. This model is based on the shear failure surface proposed by Ottosen [35] and includes the strain rate effects and strain softening in tension by incorporating crack opening width or fracture energy. The fracture energy for the concrete containing limestone aggregate, used in the experiment, was considered as 70 N/m [36]. Table 3 shows the material parameters adopted in the simulation of backfill tests.

3.4. Steel reinforcement

The steel reinforcement bars within the slab/concrete lining were modeled as beam-truss elements capable of sustaining tension and compression. Material model *MAT _PLASTIC_KINEMATIC from LS-DYNA was employed in this study as it is more efficient in terms of the computational demand. The strain rate effect is incorporated by using the Cowper Symonds strain rate model as shown in Eq. 2.

$$\sigma = \left[1 + \left(\frac{\dot{\epsilon}}{C}\right)^{\frac{1}{P}}\right]\left(\sigma_0 + \beta E_P \in_{eff}^{P}\right) \qquad \text{Eq. 2}$$

Where, σ is the dynamic flow stress at a uniaxial plastic strain rate $\dot{\epsilon}$, σ_0 is the associated flow stress, E_P is the plastic modulus and $\in_{eff}^{P}$ is the effective plastic strain of the material. This equation computes the strain rate dependent factors to scale the yield stress. Parameter β is included to differentiate the type of plastic hardening in the material model. For elastic perfectly-plastic material with kinematic hardening ($\beta = 0$) and hence the surplus stress of the plastic hardening part $\beta E_P \in_{eff}^{P}$ is omitted. C and P are strain rate parameters which were evaluated based on best fitting of the DIF of steel reinforcement as described by Malvar and Crawford [34]. This model also includes failure upon reaching a predefined value of failure strain. The material properties for the steel are described in Table 4.

Table 4: Material parameters for steel

	Density (g/cm^3)	E_s (GPa)	Poisson's ratio	σ (MPa)	E_{tan} (GPa)	β	***C*** (S^{-1})	***P***
Principal steel	7.85	200	0.3	465	2.0	0	1080	5.48
Temperature steel	7.85	200	0.3	563	2.0	0	9650	5.50
Shear steel	7.85	200	0.3	505	2.0	0	2150	5.49

3.5. Copper

The copper pipe in the centrifuge test [6] was modeled as solid elements using *MAT_PLASTIC_KINEMATIC material model. The material properties for the copper pipe

[37] are described in Table 5. The appropriate values for the strain rate parameters ***C*** and ***P*** can be found in [38].

Table 5: Material parameters for copper

Density (g/cm^3)	E_s (GPa)	Poisson's ratio	σ (MPa)	E_{tan} (MPa)	β	***C*** (S^{-1})	***P***
8.93	117	0.35	400	100	0	1.346e+06	5.286

4. Problem Description

4.1. Centrifuge test

De [6] investigated the tunnel response to a surface blast using scaled-down models with the help of a 70 g centrifuge testing machine, where g is the gravitational acceleration. The scaled-down model composed of a copper pipe buried in sand (dry Nevada sand) at a depth of 3.6 m equivalent to prototype scale. As shown in Figure 2, a sphere-shaped explosive was symmetrically positioned above the mid-span, directly over the centerline of the copper pipe, such that the ground surface was tangent to the explosive.

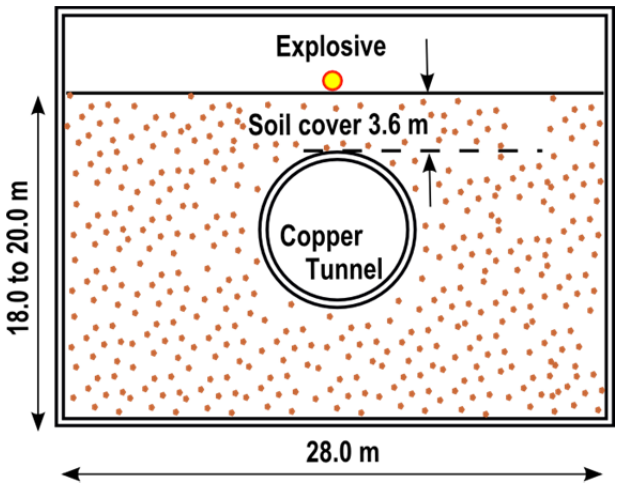

Figure 2: Experimental setup of centrifuge test (all dimensions are in prototype scale)

The response of copper pipe was monitored during the blast with strain gauges mounted to the pipe surface. Three strain gauge readings reported by De et al. [6, 39] were considered for comparison purposes. Based on the centrifuge scaling laws [40], prototype model dimensions were computed for the numerical simulation as shown in Table 6. Section 5.2 describes the corresponding gauge locations in the prototype model.

Table 6: Conversion to prototype measurements

Model Parameters	Scaled-down model dimension	Prototype model dimension
Copper pipe diameter	76 mm	5.62 m
Copper pipe thickness	2.5 mm	175 mm
Explosive weight of TNT	2.6 g	888 kg

4.2. CONWEB test (Test 3)

Four tests were conducted in the CONWEB test series [11] to investigate the backfill effects on the blast response of a buried structure shown in Figure 3. This study utilizes a test with compacted backfill sand (Test 3), where the cylindrical explosive was vertically positioned in the soil with its center aligned to the center of the structure. In this test, as illustrated in Figure 3, a 7 kg C-4 cased charge was placed 152.4 cm away from a test slab at a depth of 152.4 cm. Specimens were prepared in such a way that a reusable reaction structure was placed in an excavated test pit (6.1 m x 6.1 m x 2.4 m). The test slab was then attached to the reaction structure by means of bolts with 22.86 cm spacing along the top and bottom of the reaction structure. Backfilling was carried out with a great care to ensure the consistency of soil properties throughout the backfilling. The region outside the test pit was composed of in-situ clay. During the backfilling, a series of interface pressure gauges were installed on the other side of the charge to monitor the free-field motion of the soil. The test slab and surrounding were also instrumented to monitor the structural response as shown in Figure 4. A series of interface pressure gauges were placed as well to measure the free-field motion on other side of the charge.

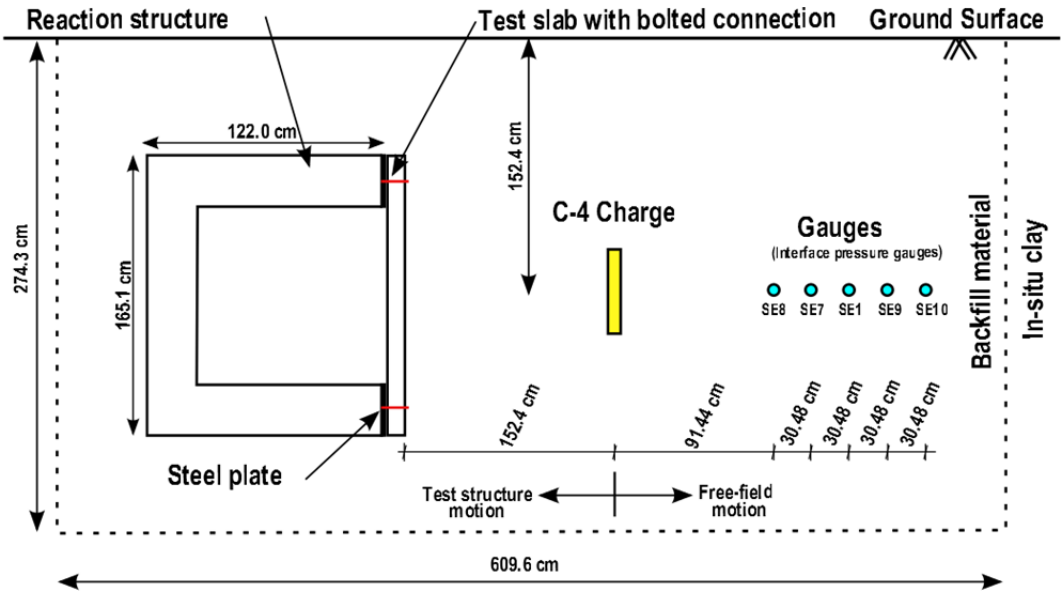

Figure 3: Experimental setup of CONWEB test

The test slab was 4.57 m in length, 1.65 m high and 10.9 cm thickness, reinforced in both vertical and horizontal directions with sufficient shear reinforcement. The reinforcement details can be found in Hayes [11]. The density and average unconfined concrete compressive strengths of the test slab concrete were 2.24 g/cm^3 and 40.4 MPa respectively. The reaction structure was a 28 cm thick heavily reinforced opened box section. The exposed surface of the reaction structure was cast with a16 mm thick steel plate which provided a hard smooth bearing interface and acts as a protective layer for the reaction structure. Section 3.2.2 describes the soil properties for this backfill.

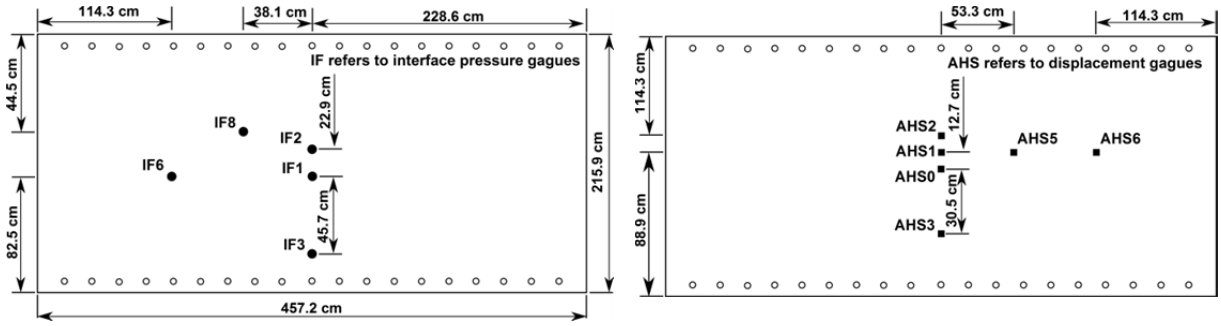

(a) Exterior face (b) Interior face with

Figure 4: Instrumentation plan of test slab

5. Numerical Simulation

5.1. Numerical model of the centrifuge test

The experimental scaled down model used by De [6] has biaxial symmetry with respect to the blast orientation. The numerical simulation utilizes the features of symmetry to model one quarter of the prototype as shown in Figure 5. Near field domain suffering large deformation was modeled with SPH particles and eight-node hexagonal solid (finite) elements were used to model the domain experiencing intermediate and small deformations. The space within the interior volume of the tunnel was specified as a vacuum.

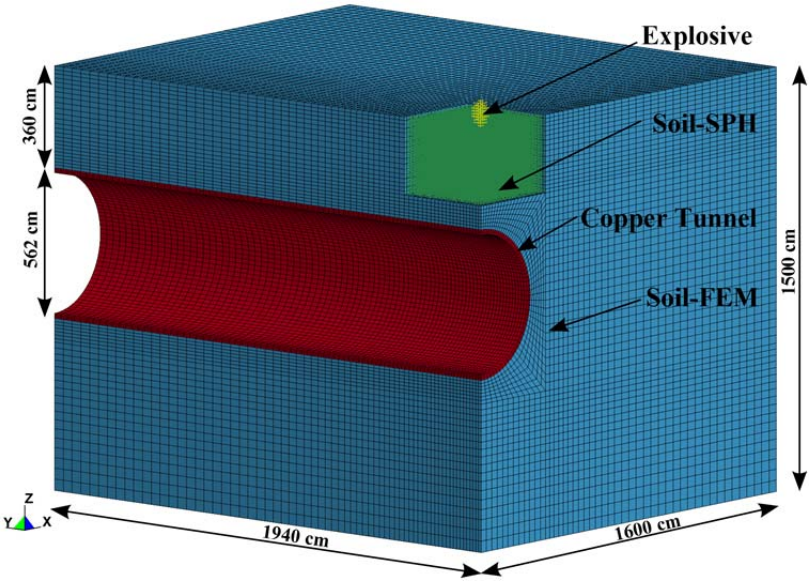

Figure 5: A quarter symmetrical numerical model

A quarter of the spherical explosive was modeled with equally spaced SPH particles. To ensure mesh consistency, SPH soil particles were modeled under the explosive within a box having the dimensions 3.50 m x 3.50 m x 2.76 m, as shown in Figure 5. All SPH particles had approximately equal inter-particle distance of 10.0 cm. A number of models with different meshes were used in a mesh refinement study to ensure mesh consistency in the numerical solution. Smaller element size of 15.0 cm x 12.5 cm x 13.0 cm was used to model the soil in the region next to the SPH soil particles, while a larger element size of 40 cm x 40 cm x 40 cm was used to model the soil in the far field domain.

The tunnel was modeled with eight-node hexagonal solid elements. In order to facilitate a nonlinear stress transfer across the thickness of the tunnel, three elements were introduced. Meshing of curvature interface between the soil and tunnel was given due considerations to avoid interlocking of elements due to peaks and valleys in the curvature. The interlocking of elements can affect the physical process with penetrating nodes and crossed edges of those elements. Therefore, a procedure was adopted to ensure that nodes on soil interface were coincident with nodes on the tunnel interface. Further refinement was made with a gradual increase in element size in both axial and circumferential directions away from the explosive. The smallest element size was 10.25 cm x 12.5 cm x 5.83 cm.

At the symmetry boundaries the nodes of the solid elements were constrained in the normal directions to the XZ and YZ planes, while a special symmetry boundary *BOUNDARY_SPH_SYMMETRY_PLANE was used for the SPH particles at these boundaries. As reflection of shock waves at the far-field boundaries affect the accuracy of the simulation, non-reflecting boundaries were employed at the furthest domain where the shock waves flow out. The bottom of the model was fixed in all directions.

Outside space of the explosive above the soil was assumed to be a vacuum which ignores the later interaction process between the explosion-produced gas and neighboring air. The interaction between the SPH and solid elements was formed by the penalty based contact *CONTACT_AUTOMATIC_NODES _TO_SURFACE. To facilitate the stress transfer with possible separation and sliding between the soil and the tunnel, *CONTACT _AUTOMATIC_SURFACE_TO_SURFACE was incorporated. Material properties for all materials were outlined in Section 3.

5.2. Numerical model of the CONWEB test

The test set up consisted of three components which are, a buried explosive, the soil and the test structure is illustrated in section 4.2. Considering the symmetries of the problem, a quarter of each of the soil and explosive and a half of the structure were modeled as shown in Figure 6 to reduce the problem size. Similar to the model in section 5.1, the explosive and near field soil media were modeled using SPH particles while the far field soil and the test structure were modeled using the eight-node hexagonal solid elements.

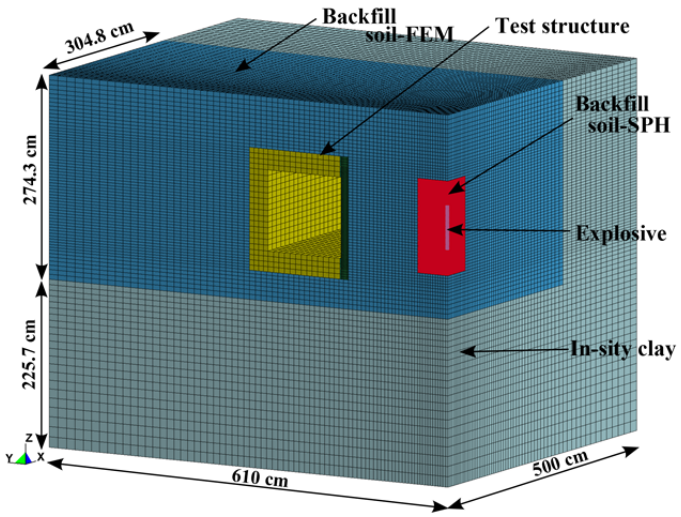

Figure 6: A half symmetrical numerical model

All SPH particles within a box of 46.5 cm x 46.5 cm x 127.5 cm were modeled with an equal inter-particle distance of 1.5 cm. A series of mesh sensitivity studies provided an appropriate mesh refinement to capture the detonation process and subsequent response of the structure. The soil was refined with a gradual increase in mesh size in both X and Y directions beyond the SPH region. The size of the smallest element adjoining the SPH region was 3.7 cm cube. Backfill soil elements were merged with the in-situ clay soil elements at the interface. Since material properties were not available for the in-situ clay, it was considered to be the same as the backfill soil. This will avoid any problems with the wave refraction/reflection at the interface of different soils and the different velocities in them.

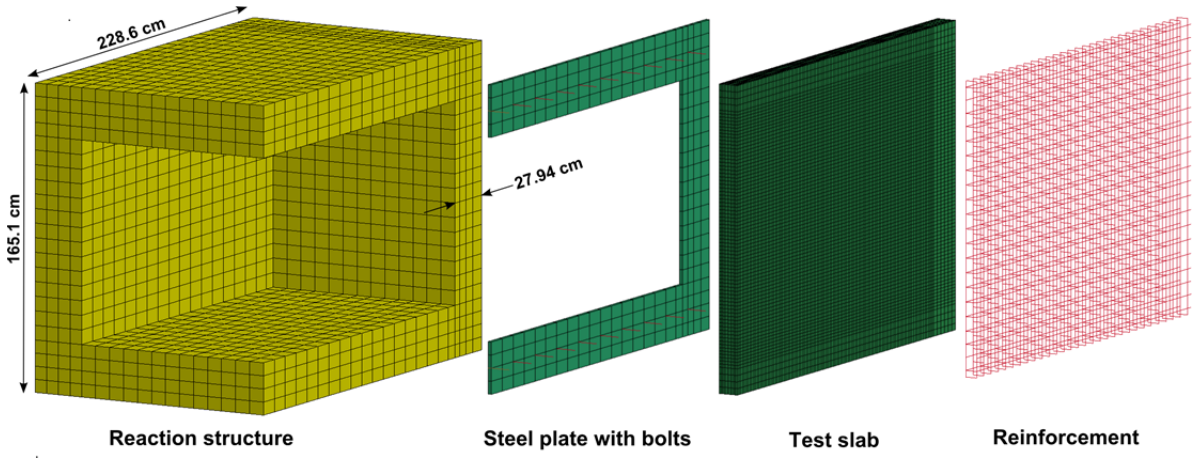

Figure 7: Reaction structure and test slab

As shown in Figure 7, half the test structure was modeled with appropriate boundary conditions at the symmetry planes. The reinforcement layout described in [11] was followed in the model where both the principal and temperature (transverse) steels were modeled discretely using truss elements with 2 x 2 Gauss integration. The shear steel and bolts were modeled as Hughes-Liu beam elements with cross sectional integration. Contact between the reinforcement and concrete was formed by merging the common nodes.

The test slab was modeled with a very fine mesh to achieve adequate accuracy in the deflection. A minimum of two hexahedral elements were specified for the reinforcement cover. There were 72960 elements in the test slab which was attached to the steel plate by 20 numbers of bolts. The bolts were modeled as discrete elements immersed in both the test slab and steel plate meshes using *CONSTRAINED_LAGRANGE_IN_SOLID coupling option. In addition, *CONTACT_AUTOMATIC_SINGLE_SURFACE contact was utilized to define the interface between the test slab and the steel plate.

Perfectly bonded ‘no slip’ condition was considered for the contact between the steel plate and reaction structure as the steel plate was cast integrally together with the reaction structure. The material properties for the steel plate were specified in [30] and the steel was associated with *MAT_PLASTIC_KINEMATIC material model. The reaction structure was a heavily reinforced concrete structure [11]. There were no reinforcement details available. For simplicity, the reaction structure was therefore modeled as a reinforced concrete structure with an equivalent stiffness, as also adopted by others [12]. Material properties for all other materials were outlined in Section 4. The boundary conditions and contacts, such as SPH particles to solid elements and soil to structure, were modeled as defined in Section 5.1.

6. Results and Discussion

All the experimental studies have been simulated using LS-DYNA R7.0.0 released in 2013. High Performance Computing (HPC) facilities at the Queensland University of Technology provide quick and accurate solutions. All simulations were conducted in two stages of stress initialization and blast analysis. Before applying the blast, models were initialized using a time-dependent mass damping option *DAMPING GLOBAL to impose near-critical damping until the preload was established.

6.1. The centrifuge test

6.1.1 Explosion and Shock wave

This simulation considered a surface explosion and subsequent response of a buried tunnel using the SPH-FEM coupling. The model was first initialized without the explosive. After initialization, the explosive SPH particles were inserted into the preloaded model and initiated the detonation at 1500 ms using the restart feature in LS-DYNA.

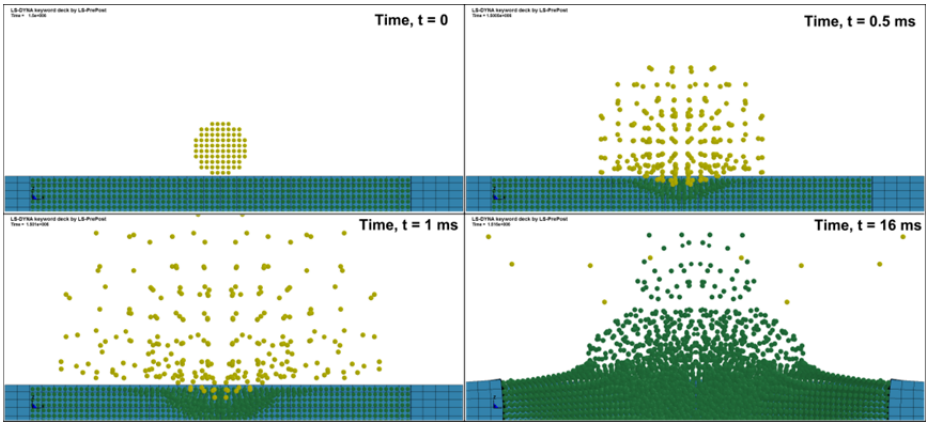

Figure 8: Explosive-soil interaction

As illustrated in Figure 8, during the explosion process, the quick interaction of the explosive with the neighboring soil SPH particles implies distortion, where those explosive SPH particles are dispersed by the flow of the expanding explosion. In the soil, the blast produced shock waves transmitted hemi-spherically through the soil and propagated at a higher rate than the crater formation as shown .in Figure 9. The shock waves reached the tunnel crown after 7 ms of the detonation. When SPH particles interacted with solid elements, the SPH-FEM coupling enabled the stress transfer at the interface without penetration of SPH particles.

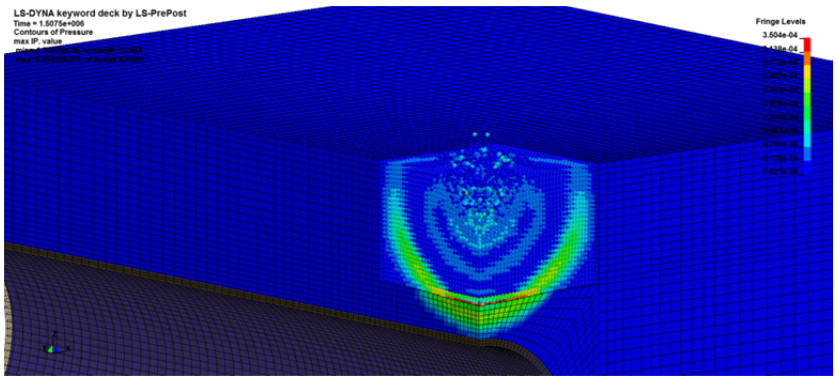

Figure 9: Shock wave propagation in soil

6.1.2 Tunnel response

The tunnel response commenced when the shock wave struck the tunnel surface. Figure 10 illustrates the interface pressure variation along the tunnel, as the shock waves progress through the soil-structure interface. The interface between the structure and the surrounding soil was simulated using thin-layer elements. Four elements were considered along the crown of the tunnel interface and Figure 11 illustrates corresponding interface pressure distributions. The peak interface pressures are high in the immediate area of the explosive. The element EL#32 experienced the highest peak pressure which is more than 600 times the geo-static stress due to the overburden soil. The peak pressure line in Figure 11 illustrates that the peak pressure drop is very high in the immediate region whereas the drop is insignificant beyond the region of element EL# 895 which is 4m from the mid-span.

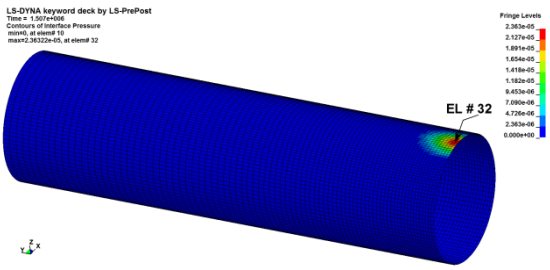

(a) t= 1507 ms

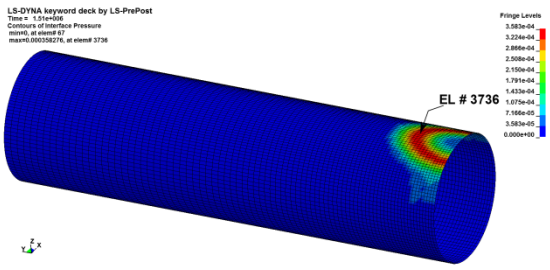

(b) t= 1510 ms

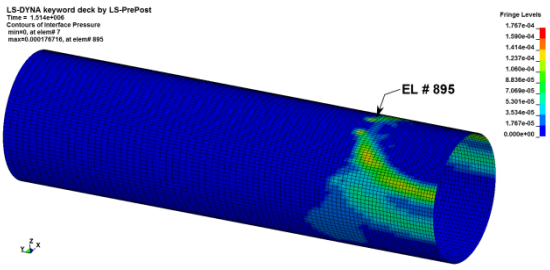

(c) t= 1514 ms

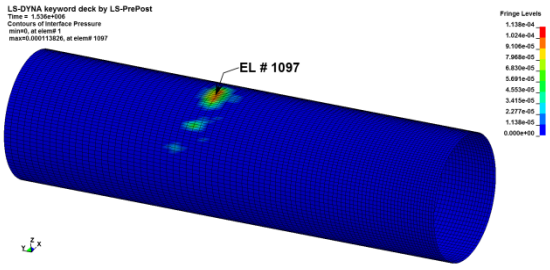

(d) t= 1536 ms

Figure 10: Interface pressure contours

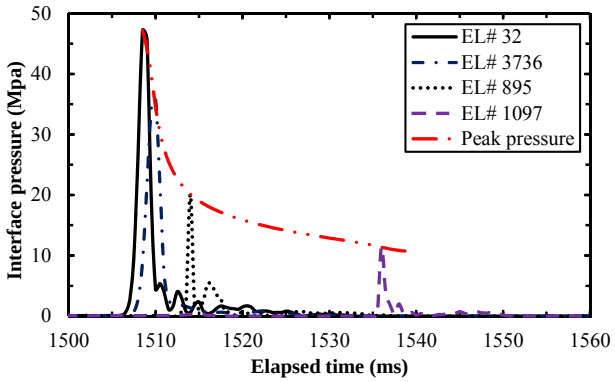

Figure 11: Interface pressure vs. time

Figures 12(a) & 12(b) illustrates the measuring points in the experiment [39] and corresponding points in the numerical model respectively. Strain gauges AS1 and AS2 were represented by Gauge 1 and Gauge 2 respectively along the surface of the tunnel crown. By considering the plane of symmetry, Gauge 3 was considered to simulate the strains in gauges CS1 and CS2 mounted on the tunnel surface on either side of the spring-line at mid-span.

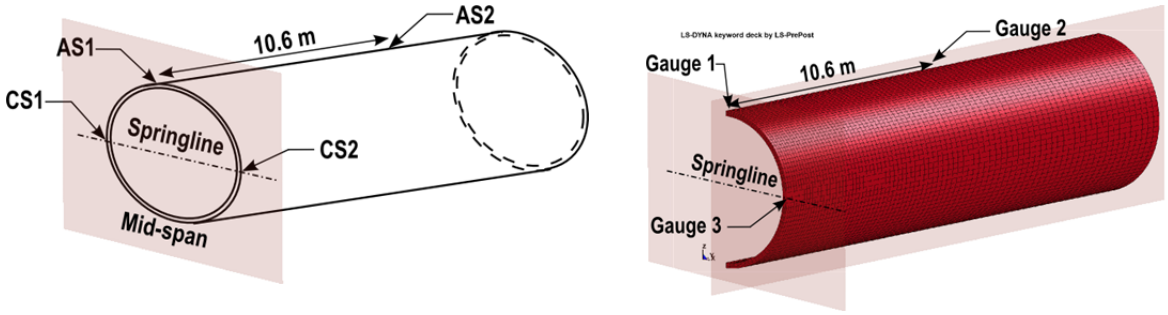

(a) Instrumentation plan in experiment

(b) Gauges in a quarter symmetric numerical model

Figure 12: Strain measuring points in experiment and numerical model

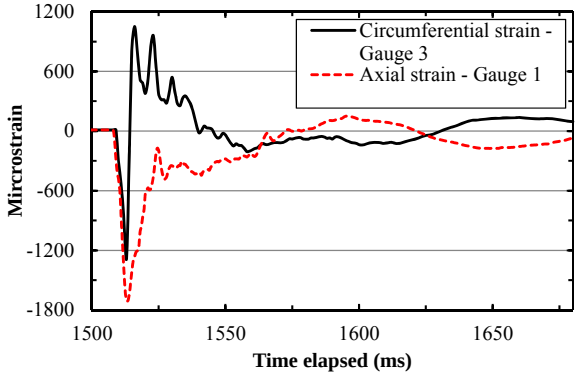

Figure 13: Axial and circumferential strains

Figure 13 displays the time histories of the axial and circumferential strains at Gauge 1 and Gauge 3 respectively. Both strain histories describe that the tunnel had largely recovered from the axial deformation at Gauge 1 and circumferential deformation at Gauge 3 although the response continued with a noticeable fluctuation after 1575 ms. Figure 14 compares the axial strain history at Gauge 2 with the corresponding strain in the centrifuge test at gauge AS2 [39]. The real-time trend curves, with closely matching peaks, describe a reasonable good correlation between the numerical and the experimental results.

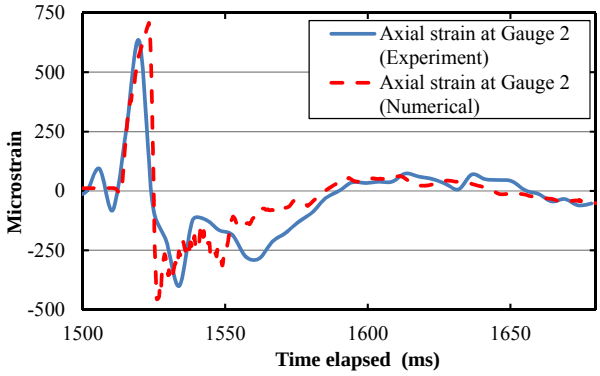

Figure 14: Axial strain comparison at Gauge 2

In the present study, the variation of the peak strain vs. scaled distance was obtained by varying explosive masses and the results are shown in Figure 15. In Figure 15(a), peak axial strain at Gauge 1 was compared with that from the centrifuge test [6]. The comparison shows a small variation which was also observed in the numerical simulations described by De [6]. The discrepancy could be explained by the confinement effect of the test-bucket. In an infinite soil domain, the tunnel has no movement restrictions. Furthermore, the assumption of the explosive surrounded by a vacuum ignored the interaction between the explosive and air. This could overestimate the tunnel response in the numerical simulation.

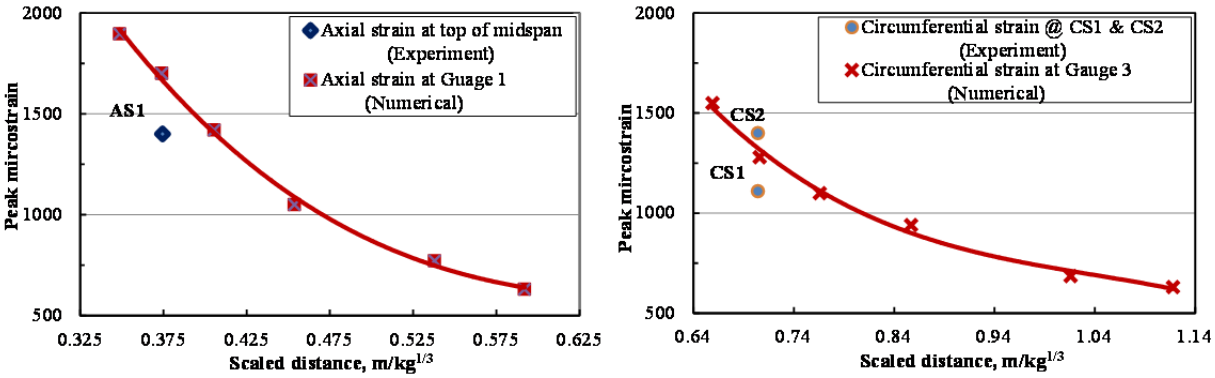

(a) Comparison of peak axial strains

(b) Comparison of peak circumferential strains

Figure 15: Comparison of peak axial and circumferential strains

Figure 15(b) shows the comparison of the circumferential strains at Gauge 3 with the experimental results at both CS1 and CS2. Although these two experimental results showed a significant gap, the comparison shows that the numerical best-fit line lies within those two experimental values.

6.2. The CONWEB test

6.2.1 Free-field analysis

Free-field analysis was performed to evaluate a best fit material parameter of PWD1 which is one of the parameters used to incorporate the pore water effects in the soil. In this numerical simulation, the charge was modeled using SPH particles without the casing as SPH is incapable of modeling shell elements. Figure 16 shows the comparison of peak pressure from the present numerical study with those from the CONWEB free-field test [11] for partially saturated sand. It can be seen that the best fit line of the sand has a perfect match with the measured free-field peak pressure and it also complies with a linear power law on a logarithmic scale. The free-field simulation therefore agreed reasonably well with the test results and provides a means to evaluate the best fit PWD1parameter for the partially saturated sand as 25.0 GPa^{-1}.

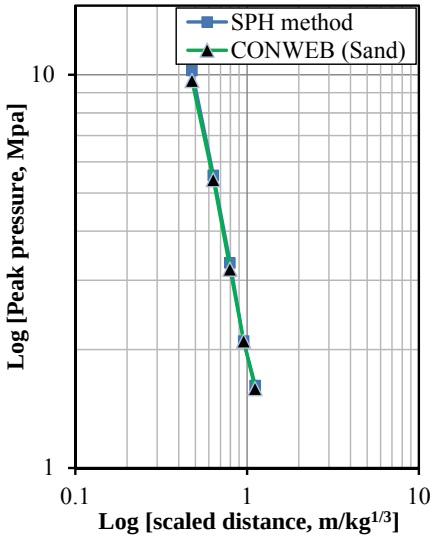

Figure 16: Comparison of peak pressures

6.2.2 Test slab response

After initializing the model, the explosive was detonated. The explosion induced shock waves traveled through the soil. The structure began to respond when the shock waves reached the soil structure interface. Figure 17 illustrates the variation of interface pressure contours at the interface of the soil structure.

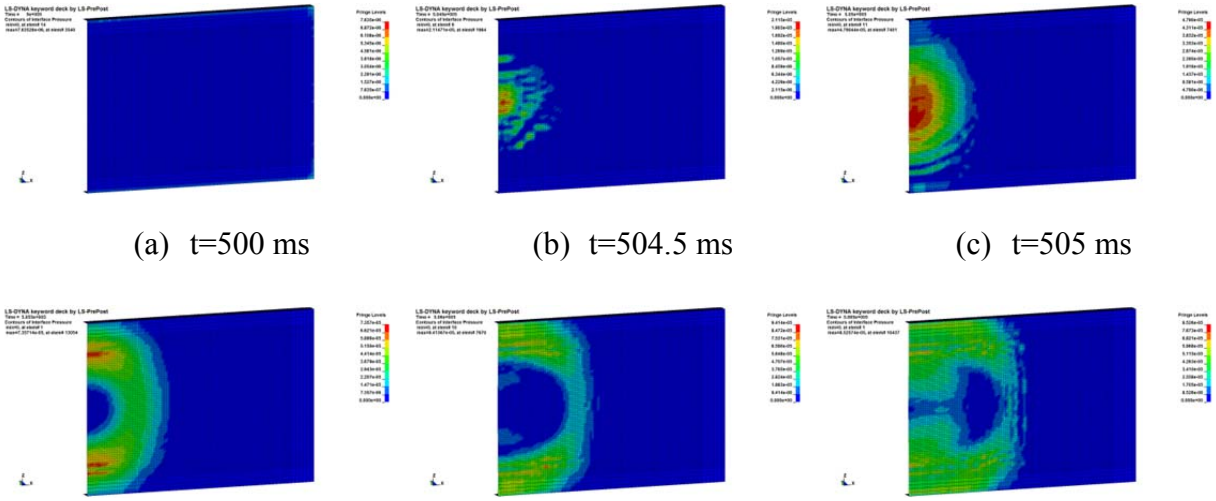

(a) t=500 ms (b) t=504.5 ms (c) t=505 ms

(d) t=505.5 ms (e) t=506 ms (f) t=506.5 ms

Figure 17: Interface pressure contours for Mat_rel3

The peak pressure which results from the interaction of the structure and the surrounding soil is the dominant parameter that influences the response of the test slab. This peak interface

pressure was therefore considered in the present study. In Figure 18, the peak interface pressures obtained by using both the Mat_rel3 and the Mat_winfr concrete material models are compared with those obtained from the test. The peak pressures evaluated by using the Mat_winfr concrete model agree better with those from the experiment at many locations compared to those obtained by using Mat_rel3 concrete model.

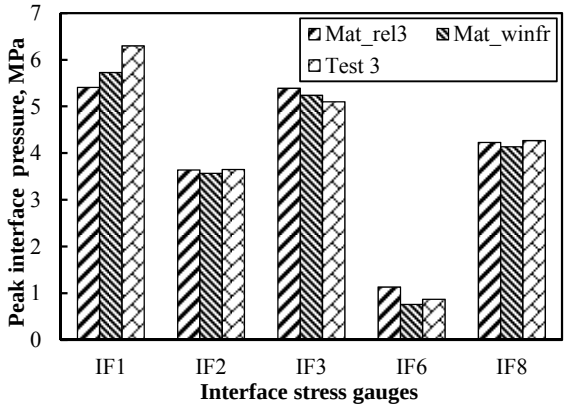

Figure 18: Comparison of peak interface pressures

The response the test slabs under blast load was investigated. Both material models showed a similar kind of breaching failure at the center of the test slab and the failure extended away from the center. Shear failure was observed at the end support along the floor and roof edges of the reaction structure. A separation between the test slab and steel plate was also observed due to both localized rotation along the support edges and straining of bolts. The effective plastic strain contours shown in Figure 19(a)-(c) represent the damage level that the test slab experienced in this simulation using Mat_rel3 concrete model. This shows that the test slab suffered severe damage in a very short period of time. Figure 19(d)-(f) shows the simulation results using Mat_winfr model for the concrete. Failure of the concrete is illustrated by the formation of cracks. During early stages of the simulation, cracks were vertical and parallel to the principal steel. At later stages of the simulation, number of diagonal cracks emanated from the bolt locations. Comparisons of the interior view of the test slab damage [11] and numerical simulations illustrate that the damage patterns at the interior face of the slab are similar in both simulations. However, the simulation using Mat_rel3 considerably over estimates the damage in terms of qualitative assessment.

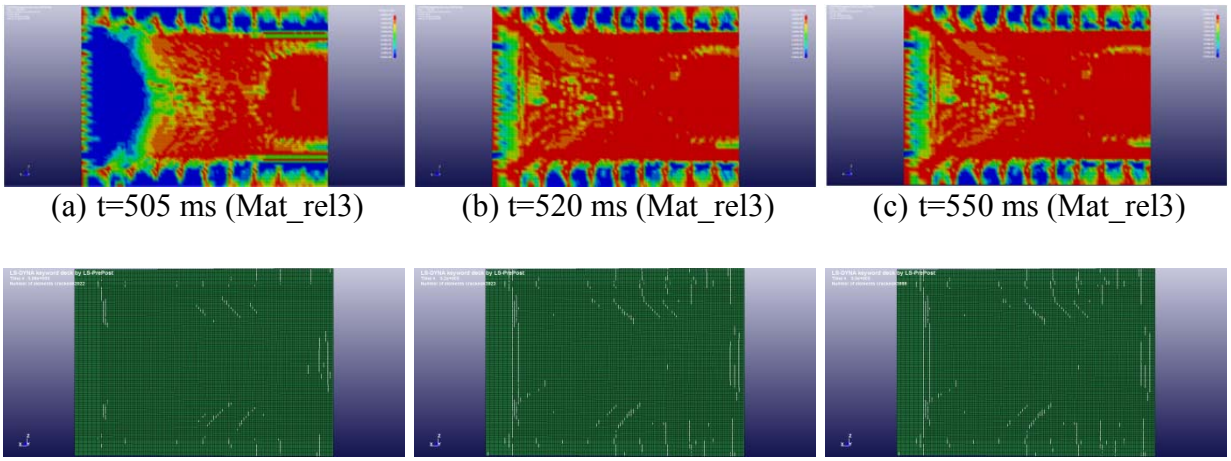

(a) t=505 ms (Mat_rel3) (b) t=520 ms (Mat_rel3) (c) t=550 ms (Mat_rel3)

(d) t=505 ms (Mat_winfr) (e) t=520 ms (Mat_winfr) (f) t=550 ms (Mat_winfr)

Figure 19: Comparison of failure patterns

Finally, the displacement histories of six gauges are compared as shown in Figure 20. A slight lag in the time-of-arrival was clearly observed in both simulations. This lag could be attributed to a lack of adequate soil material properties which were evaluated by several assumptions and empirical formulae. At several locations, Mat_rel3 over-predicted the deflections when compared to the deflection obtained from the experiment. In Mat_rel3, gauges AHS-1, AHS-5 and AHS-6 below the center line of the slab showed about a 10% increase in deflection when compared with the experiment. Gauges AHS-0, AHS-1 and AHS-2 in the immediate region responded with a steep slope compared to the experimental slope which represented the velocity in the displacement-time plot. Though the deflections obtained from Mat_winfr were less than those observed in the experiment, the predictions of final displacements were closer to the experimental results at many locations. Overall, for this experimental configuration, concrete model Mat_winfr provides better results with respect to interface pressure, crack propagation and deflection than the concrete mode Mat_rel3.

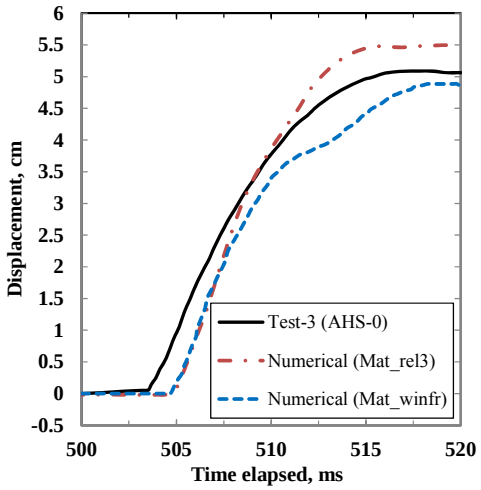

(a) AHS-0

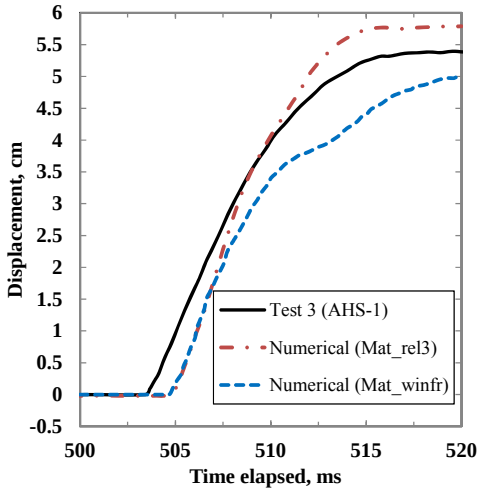

(b) AHS-0

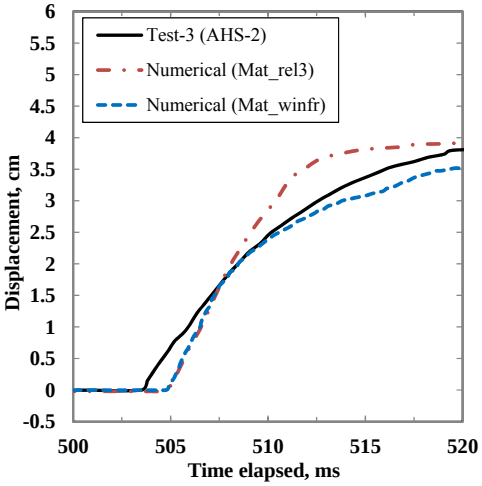

(c) AHS-2

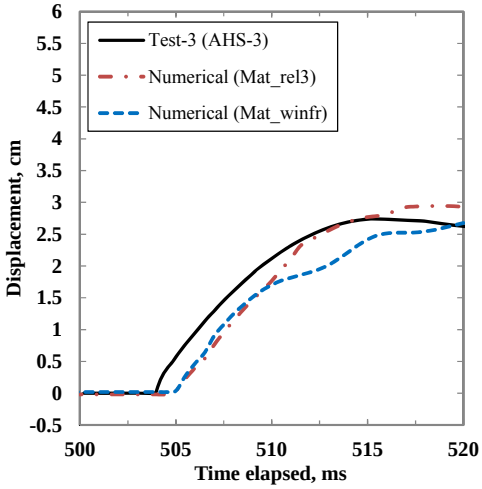

(d) AHS-3

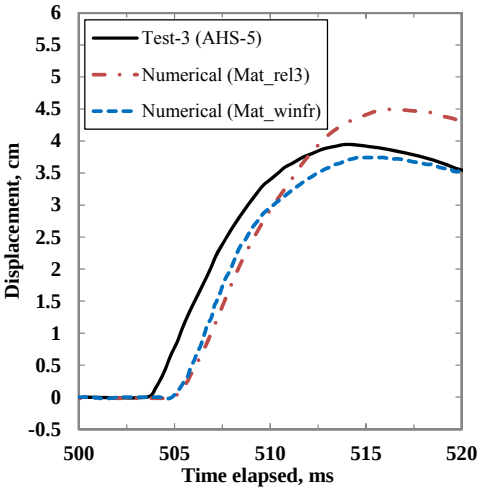

(e) AHS-5

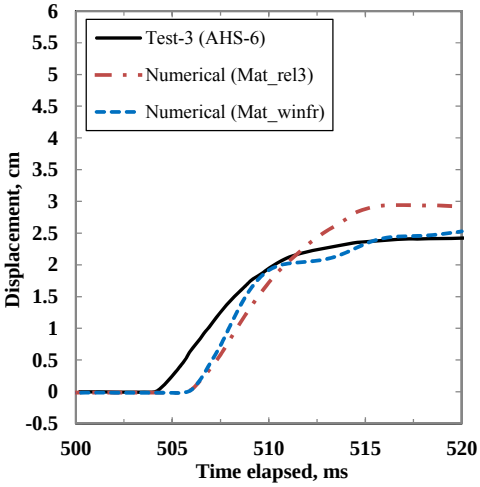

(f) AHS-6

Figure 20: Comparison of displacements

7. Parametric study on the segmented bored tunnel

Numerical techniques validated with the above two experiments provide confidence in investigating the failure of a segmented bored tunnel. This section treats the effects of explosive weight on the shallow tunnels buried in ‘dry’ sand. Cylindrical TNT explosives were buried below the ground surface as shown in the quarter symmetric model in Figure 21.

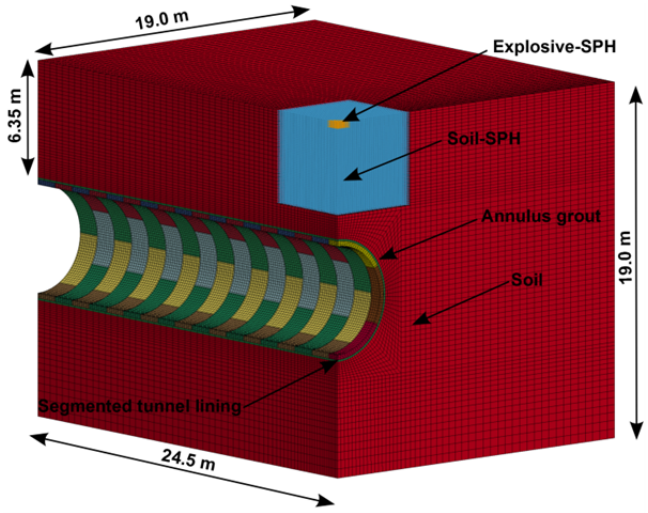

Figure 21: A quarter symmetrical model with segmented lining

As described in Figure 22(a), a common single tube railway tunnel system [41] was considered with a 150 mm thickness annulus concrete grout around the tunnel. Six identical segments were introduced to complete one lining ring (width of 1.4 m) to span the circumference of the tunnel. The segments were reinforced concrete with a concrete cover of 40 mm, as shown in Figure 22(b). Bolts (M24 bolt grade 8.8) were used in both radial and circumferential directions of joint segments as displayed in Figure 22(c) and (d).

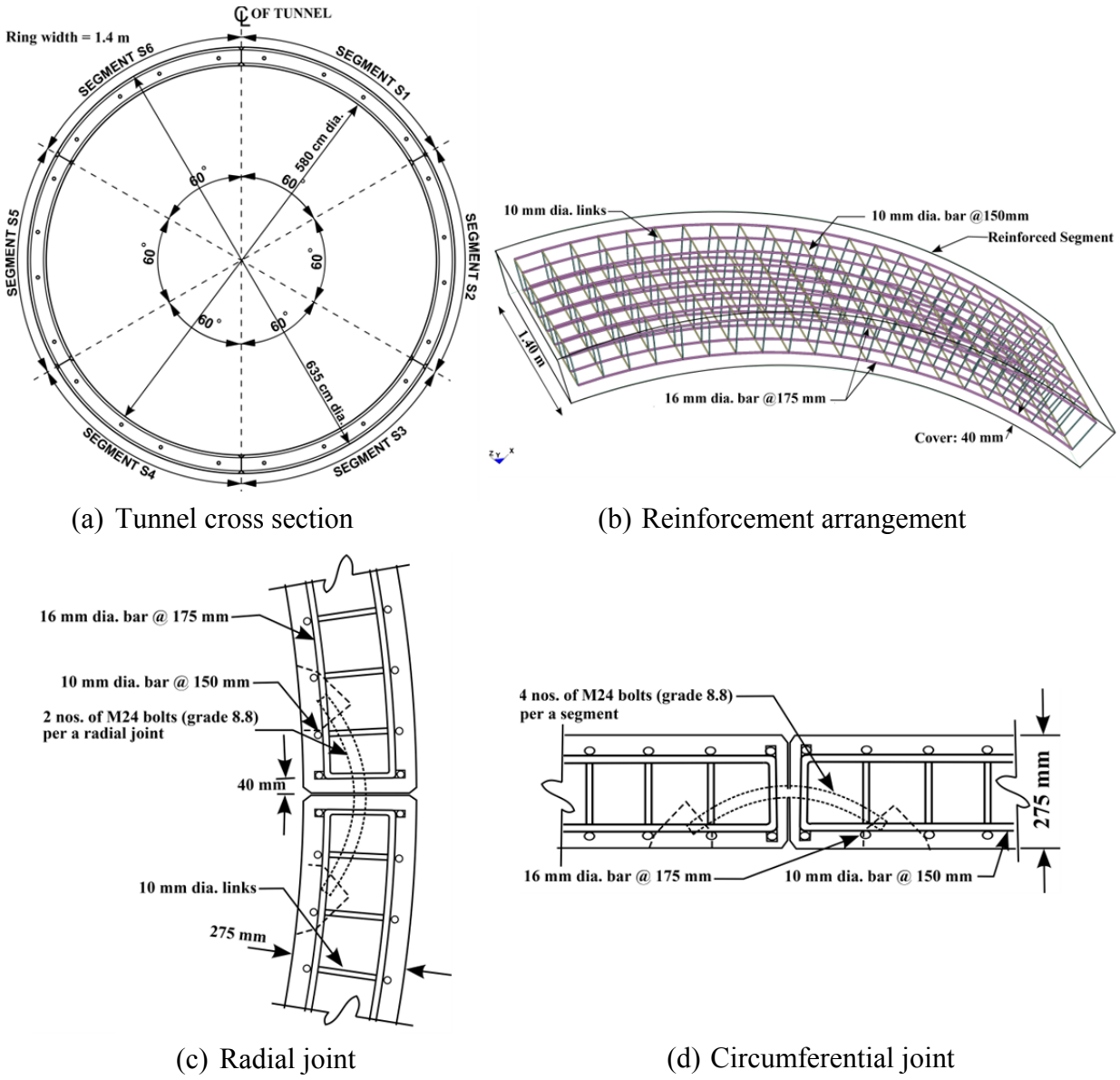

(a) Tunnel cross section (b) Reinforcement arrangement

(c) Radial joint (d) Circumferential joint

Figure 22: Segmented bored tunnel

In order to examine the effect of explosive weight for a given value of the tunnel crown cover, five load cases were considered, as shown in Table 7. For the range of credible medium blast loading, the study focused on the drift or relative transverse displacement between segmented lining rings and failure of the segments in three dimensions.

Table 7: Load cases

Case	1	2	3	4	5
TNT explosive, (kg)	253	389	544	758	1010

As the shock waves traveled through the tunnel, ovaling of the tunnel profile was observed in the lining ring. Within the lining ring, segments responded in an arch like behavior that directly transferred the load to adjoining segments through the radial joints. In the longitudinal direction, the vertical component of the blast load redistributed to its adjacent segments through the shear force transmission capacity at the circumferential joints. The lateral component of the blast load was transferred to the neighboring rings by compressing the segments in the longitudinal direction as the shock waves progressed. The results showed that the circumferential joints were more susceptible to failure than radial joints under the medium explosive range.

The longitudinal view of the tunnel in Figure 23(a) shows the drift between adjacent lining rings at the tunnel crown for load case 5. It was observed that vertical displacements at the tunnel crown decrease with the distance from the explosive. As a result of shearing of bolts at the circumferential joints, the tunnel profile displayed sudden drops in displacement between subsequent lining rings (drift). The shearing, in turn, generated tensile stress that initiated localized failure in the segments. Figure 23(b) compares the tunnel drifts at a critical interface (closest to the explosive) for load cases 1 to 5. As expected, the drift increases with explosive weight. In load case 1, there were no failure of bolts and the drift was recovered. Load cases 2 to 5, however, generated a permanent drift which may be sufficient to damage the gasket placed between the segments. Bolts are critical for alignment control and water-tightness in the tunnel lining. Failure of many bolts in load cases 4 and 5 amplified shearing displacement which may cause the soil and water inflow into the tunnel.

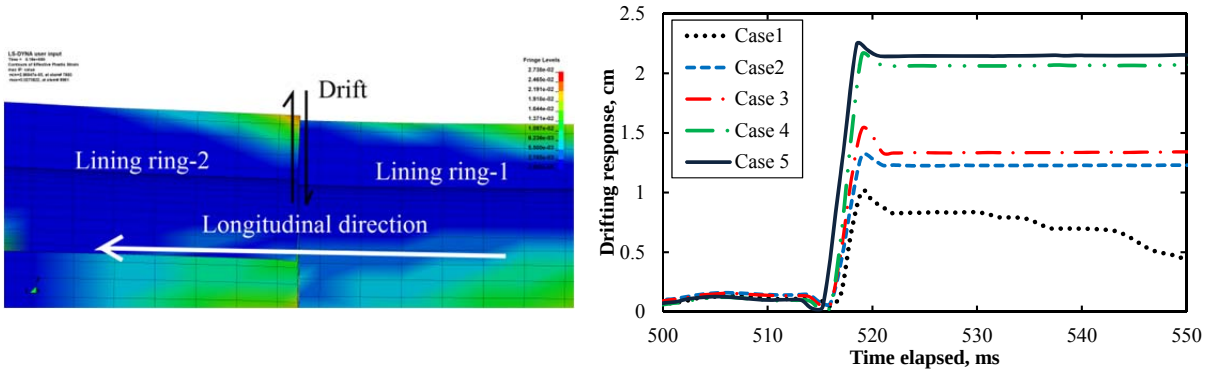

(a) Drift between lining rings (b) Drifting response

Figure 23: Drifts between segmented lining rings

The lining ring that was closest to the explosive ruptured first with cracks and a significant number of progressive cracks developed during the phase of lining vibration following the blast. Cracks were mainly generated by bending stresses and the number of cracks increased with explosive. Figure 24 shows the cracks induced after 17 ms of detonation in load case 3. In the proximity to the tunnel crown as shown in Figure 24(a), the flexural cracks was first triggered by residual circumferential stresses from the combined action of hoop stresses and circumferential bending stresses on the interior surface of the segments. As displayed in Figure 24(b), further flexural cracks developed on the top surface of the segments due to the similar action, but the bending stresses were on the exterior surface. The main cracks that appeared in the longitudinal direction have the expectable orientation due to the bending stresses produced in the circumferential direction according to the ring-arch mechanism.

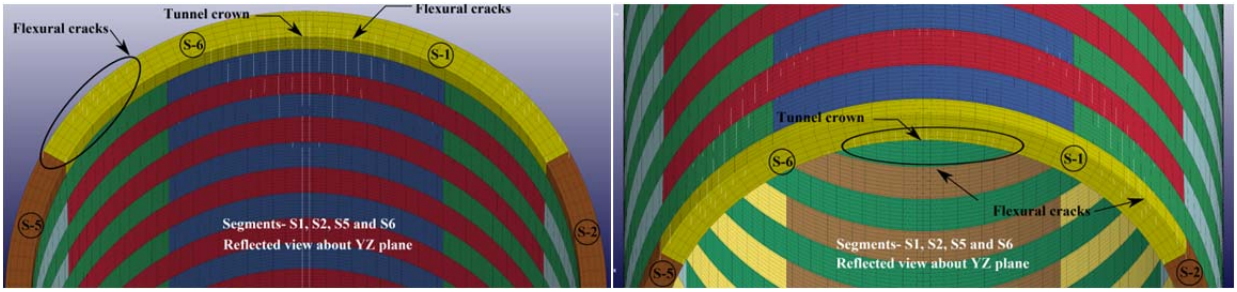

(a) View of cracks in the tunnel interior (b) External view of cracks

Figure 24: Crack patterns obtained from numerical simulations

Figure 25 compares the vertical displacement history of a point closest to the tunnel crown for load cases 1 to 5. Underground transportation deserves high level of safety in terms of the degree of structural performance. Excessive displacement of the tunnel elements poses a hazard for the operational envelope, in which train and other services are accommodated. Displacement under load case 1 may be marginally adequate for the train to escape from the tragedy. However, peak displacement computed from load cases 3 to 5 highlights the possible structural collapses which may cause catastrophic train crashes. The drift between the rings accelerates the soil and water inflow which may make the situation even worse by affecting the integrity of the above ground structures.

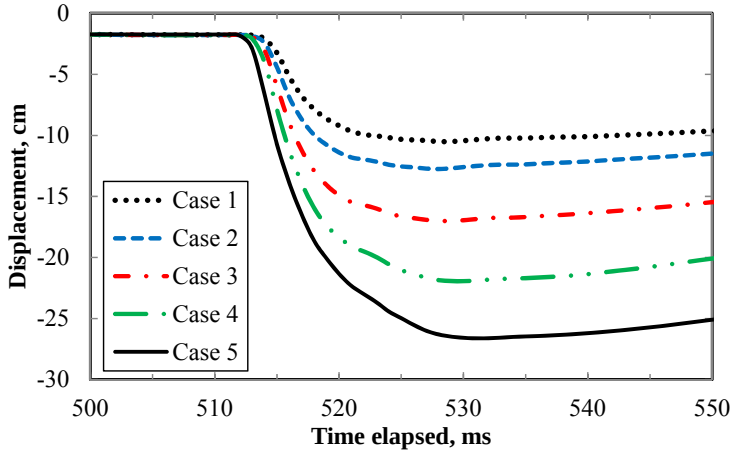

Figure 25: Tunnel responses for different load cases

By comparing the results under the different load cases, it seems that the tunnel may be safe under load case 1 although the crack exceeded the limiting value of 0.3mm.

8. Conclusion

A fully coupled technique incorporating the Smooth Particles Hydrodynamics (SPH) method and the Finite Element Method (FEM) was developed and applied to investigate the blast response of a segmented buried tunnel using the software LS-DYNA. This innovative research involved the application of appropriate coupling mechanism between the SPH particles and the Finite Elements and choice of appropriate material models. The modeling techniques were validated using results from experiments involving above and below ground explosions. This provides confidence in applying the developed techniques to treat the blast response of segmented bored tunnels and the influence of important parameters.

The general behavior of the segmented tunnel response was demonstrated for various load cases. The results showed that the tunnel rings responded as arch mechanisms under the blast load and they redistributed the blast load to the adjacent rings through the circumferential joints. In these joints, many bolts in the vicinity of the explosive had failed. However, bolts at the radial joints were sustained by the hoop stress. The drift responses between lining rings, crack patterns and vertical displacements provide new and useful information in the area of blast response of segmented tunnels and will provide guidance in future modeling and analysis in this area.

References

[1] V.R. Feldgun, A.V. Kochetkov, Y.S. Karinski, D.Z. Yankelevsky. Internal blast loading in a buried lined tunnel International Journal of Impact Engineering 35 (2008) 172 - 83.
[2] H. Liu. Soil-Structure Interaction and Failure of Cast-Iron Subway Tunnels Subjected to Medium Internal Blast Loading. Journal of Performance of Constructed Facilities. Vol. 26 (2012) 691-701.
[3] H. Liu. Dynamic Analysis of Subway Structures Under Blast Loading. Geotechnical and Geological Engineering. 27 (2009) 699-711.
[4] P.E. Nasri Munfah. SAFETY AND SECURITY OF TUNNELS AND UNDERGROUND TRANSPORTATION FACILITIES. Parsons Brinckerhoff, National Tunnelling Practice Leader, New York, USA. (2009).
[5] A. De, A.N. Morgante, T.F. Zimmie, Mitigation of Blast Effects on Underground Structure Using Compressible Porous Foam Barriers, Poromechanics V, 2013, pp. 971-80.
[6] A. De. Numerical simulation of surface explosions over dry, cohesionless soil. Computers and Geotechnics. 43 (2012) 72-9.
[7] M.C.R. Davies, Dynamic Soil Structure Interaction Resulting from Blast Loading, in: C.F. Leung, F.H. Lee, T.S. Tan (Eds.), Centrifuge 94. Rotterdam:Balkema, 1994, pp. 319-24.
[8] M.C.R. Davies, A.J. Williams. Centrifuge Modelling the Protection of Buried Structures Subjected to Blast Loading. Structures Under Shock and Impact II. (1992) 663-74.
[9] B.L. Kutter, L.M. O'Leary, P.Y. Thompson. GRAVITY-SCALED TESTS ON BLAST-INDUCED SOIL-STRUCTURE INTERACTION. Journal of Geotechnical Engineering,. 114 (1988) 431-47.
[10] J.P. Whittaker, Centrifugal and numerical modeling of buried structures. Volume 3. A centrifuge study of the behavior of buried conduits under airblast loads. Final report, Colorado Univ., Boulder (USA). Dept. of Civil, Environmental, and Architectural Engineering, 1987.
[11] P.G. Hayes, Backfill Effects on Response of Buried Reinforced Concrete Slabs, Waterways Experiment Station, Corps of Engineers, Vicksburg, Mississippi, 1989.
[12] Y. Yang, X. Xie, R. Wang. Numerical simulation of dynamic response of operating metro tunnel induced by ground explosion. Journal of Rock Mechanics and Geotechnical Engineering. (2010) 373-84.
[13] M. Gui, M. Chien. Blast-resistant Analysis for a Tunnel Passing Beneath Taipei Songshan Airport–a Parametric Study. Geotechnical and Geological Engineering. 24 (2006) 227-48.
[14] L. Laine, A. Sandvik. Derivation of Mechanical properties for sand. Proceedings of the 4th Asia-Pacific Conference on Shock and Impact Loads on Structures, CI-Premier PTE LTD, Singapore. (2001) 361-8.
[15] LSTC. LS-DYNA Keyword User's Manual v971, Livermore Software Technology Corporation(LSTC). California, USA. (2007).
[16] L. Lucy. A numerical approach to the testing of the fission hypothesis. The Astronomical Journal. 82 (1977) 1013-24.

[17] R.A. Gingold, J.J. Monaghan. Smoothed particle hydrodynamics-theory and application to non-spherical stars. Monthly Notices of the Royal Astronomical Society. 181 (1977) 375-89.
[18] J.J. Monaghan. Simulating Free Surface Flows with SPH. Journal of Computational Physics. 110 (1994) 399-406.
[19] J.J. Monaghan. Smoothed particle hydrodynamics. Annual review of astronomy and astrophysics. 30 (1992) 543-74.
[20] I. Thiyahuddin, Y. Gu, D.P. Thambiratnam, A coupled SPH/FEM analysis of portable water filled barriers, 4th International Conference on Computational Methods (ICCM2012), Gold Coast, Qld., 2012.
[21] Z. Wang, Y. Lu, H. Hao, K. Chong. A full coupled numerical analysis approach for buried structures subjected to subsurface blast. Computers & Structures. 83 (2005) 339-56.
[22] J. Wang, Aeronautical, M.R. Laboratory, D. Science, T.O. Aeronautical, M.R. Laboratory, et al. Simulation of Landmine Explosion Using LS-Dyna3d Software: Benchmark Work of Simulation of Explosion in Soil and Air. DSTO Aeronautical and Maritime Research Laboratory, 2001.
[23] B.A. Lewis, Manual for LS-DYNA Soil Material Model 147, Federal Highway Administration, McLEAN, VA, 2004.
[24] M. Saleh, L. Edwards, Application of a soil model in the numerical analysis of landmine interaction with protective structures 26th International symposium on blastics MIAMI, FL, 2011.
[25] A.J. Abbo, S.W. Sloan. A smooth hyperbolic approximation to the Mohr-Coulomb yield criterion. Computers & Structures. 54 (1995) 427-41.
[26] L.B. Jayasinghe, D.P. Thambiratnam, N. Perera, J.H.A.R. Jayasooriya. Computer simulation of underground blast response of pile in saturated soil. Computers & Structures. 120 (2013) 86 - 95.
[27] W.Y. Lee. Numerical modeling of blast-induced liquefaction: Department of Civil and Environmental Engineering, Brigham Young University; 2006.
[28] Ortman, M. Catherine, The Effect of Diameter on Dynamic Seabed Penetration, NAVAL ACADEMY ANNAPOLIS MD, 2008.
[29] K. Arulmoli, V. Project, E.T. Corporation, N.S. Foundation. VELACS Verification of Liquefaction Analyses by Centrifuge Studies Laboratory Testing Program: Soil Data Report. Earth Technology Corporation, 1992.
[30] G.C. Bessette, Modeling Coupled Blast/Structure Interaction with Zapotec, Benchmark Calculations for the Conventional Weapon Effects Backfill (CONWEB) Tests, Sandia National Laboratories Report SAND20044096, 2004.
[31] J.T. Baylor, Parameters Affecting Loads on Buried Structures Subjected to Localized Blast Effects, Army Engineer Waterways Experiment Station Vicksburg Ms Structures Lab, 1992.
[32] L.E. Schwer, L.J. Malvar. Simplified concrete modelling withMat_Concrete_Damage_REL3. JRI LS-DYNA User Week (2005).
[33] L.J. Malvar, J.E. Crawford, J.W. Wesevich, D. Simons. A plasticity concrete material model for DYNA3D. International Journal of Impact Engineering. 19 (1997) 847-73.

[34] L.J. Malvar, J.E. Crawford, Dynamic Increase Factors for Concrete, Twenty-Eight DDESB Seminar, Orlando, FL,, August 1998.
[35] N.S. Ottosen. A Failure Criterion for Concrete. Journal of Engineering Mechanics Division. 103 (1977) 527-35.
[36] D. Darwin, S. Barham, R. Kozul, S. Luan. Fracture energy of high-strength concrete. ACI Materials Journal. 98 (2001).
[37] D.A. Matuska, HULL Users' Manual, DTIC Document, 1984.
[38] M. Peroni, L. Peroni, A. Dallocchio, Thermo-mechanical model identification of a strengthened copper with an inverse method, DYMAT 2009-9th International Conference on the Mechanical and Physical Behaviour of Materials under Dynamic Loading, 2009, pp. 1367-73.
[39] A. De, T.F. Zimmie, Modeling of Surface Blast Effects on Underground Structures, Geotechnical Engineering in the Information Technology Age Proceedings of GeoCongress;, 2006.
[40] Kramer. Geotechnical Earthquake Engineering. Pearson Education, 1996.
[41] Dazhi Wen, John Poh, Y.W. Ng. Design considerations for bored tunnels at close proximity. Tunnelling and Underground Space Technology. 19 (2004) 468-9.